LIMNOLOGY and OCEANOGRAPHY

ASLO

Limnol. Oceanogr. 9999, 2020, 1–13

doi: 10.1002/lno.11594

The role of photomineralization for CO_2 emissions in boreal lakes along a gradient of dissolved organic matter

Lina Allesson,[1*] **Birgit Koehler**,[2] **Jan-Erik Thrane**,[3] **Tom Andersen**,[1] **Dag O. Hessen**[1]

[1]Department of Biosciences, University of Oslo, Oslo, Norway
[2]Department of Ecology and Genetics/Limnology, Uppsala University, Uppsala, Sweden
[3]Norwegian Institute for Water Research, Oslo, Norway

Abstract

Many boreal lakes are experiencing an increase in concentrations of terrestrially derived dissolved organic matter (DOM)—a process commonly labeled "browning." Browning affects microbial and photochemical mineralization of DOM, and causes increased light attenuation and hence reduced photosynthesis. Consequently, browning regulates lake heterotrophy and net CO_2-efflux to the atmosphere. Climate and environmental change makes ecological forecasting and global carbon cycle modeling increasingly important. A proper understanding of the magnitude and relative contribution from CO_2-generating processes for lakes ranging in dissolve organic carbon (DOC) concentrations is therefore crucial for constraining models and forecasts. Here, we aim to study the relative contribution of photomineralization to total CO_2 production in 70 Scandinavian lakes along an ecosystem gradient of DOC concentration. We combined spectral data from the lakes with regression estimates between optical parameters and wavelength specific photochemical reactivity to estimate rates of photochemical DOC mineralization. Further, we estimated total in-lake CO_2-production and efflux from lake chemical and physical data. Photochemical mineralization corresponded on average to 9% ± 1% of the total CO_2-evasion, with the highest contribution in clear lakes. The calculated relative contribution of photochemical mineralization to total in-lake CO_2-production was about 3% ± 0.2% in all lakes. Although lakes differed substantially in color, depth-integrated photomineralization estimates were similar in all lakes, regardless of DOC concentrations. DOC concentrations were positively related to CO_2-efflux and total in-lake CO_2-production but negatively related to primary production. We conclude that enhanced rates of photochemical mineralization will be a minor contributor to increased heterotrophy under increased browning.

Most lakes worldwide are supersaturated with carbon dioxide (CO_2), emitting 0.32–0.53 Pg CO_2-C yr^{-1} to the atmosphere on a global scale (Cole et al. 2007; Raymond et al. 2013). A major part of the CO_2 emitted from lakes is produced through mineralization of dissolved organic matter (DOM) (Vachon et al. 2016). DOM in freshwaters originates both from in situ primary production and from the surrounding terrestrial ecosystems, with a general dominance of the latter (Karlsson et al. 2009). Terrestrially derived DOM consists primarily of high molecular weight humic substances. These substances make the majority of the dissolved organic carbon (DOC) pool in most lakes and thus we will primarily refer to DOC, hence using C as a common currency, through the following text. DOC poses a multitude of partly contrasting impacts on the physical and chemical properties of water, as well as on the biota (Hessen and Tranvik 1998).

Humic substances are a major source of energy to heterotrophs in aquatic ecosystems with high terrestrial influence and the subsequent increase in heterotrophic CO_2 production may indirectly stimulate autotrophs. Nutrients associated with DOC may stimulate both heterotrophic and autotrophic productivity in nutrient-poor regions. Further, humic substances are often highly aromatic and can protect aquatic organisms from harmful UV-radiation (Dillon and Molot 2005; Kritzberg and Ekström 2011). On the other hand, at a certain threshold concentration (possibly around 5 mg l^{-1}; Seekell et al. 2015), terrestrial DOC may shift from acting as a nutrient subsidy to suppressing primary production due to light attenuation (Thrane et al. 2014; Seekell et al. 2015). Lakes with high inputs of terrestrial DOC are often to a larger degree supersaturated with CO_2 than lakes where the major part of the DOC pool originates from in-lake production (Cole et al. 2000; Larsen et al. 2011*a*).

*Correspondence: lina.allesson@ibv.uio.no

Additional Supporting Information may be found in the online version of this article.

Besides being an essential source of energy for bacterioplankton (Hessen 1992), this terrigenous DOC is highly chromophoric and photo-reactive, especially in the UV waveband (Lindell et al. 1995). Photomineralization of DOC to dissolved inorganic carbon (DIC) might therefore be a significant part of the DIC production and carbon cycling in humic lakes, adding to the high respiratory activity of heterotrophic prokaryotes and low autotrophic CO_2-fixation. The annual photochemical mineralization has been estimated to account for 9–12% of the total lake CO_2 emission in the boreal biome, and amount to 13–35 Tg C yr^{-1} from inland waters worldwide (Koehler et al. 2014). However, the relative contribution of photochemical mineralization to in-lake carbon cycling varies significantly both between systems (Granéli et al. 1996; Molot and Dillon 1997; Cory et al. 2014) and temporally within the same system (Groeneveld et al. 2016; Vachon et al. 2016).

In order to simulate photochemical mineralization, knowledge of the reactivity across the whole spectrum of photochemically active wavelengths is needed. This photochemical reactivity or apparent quantum yield (AQY) of DIC photoproduction is defined as moles photochemically produced DIC per mole photons absorbed by the DOC pool (Miller et al. 2002). Besides the quantity of DOC, studies have found photochemical DIC production rates to be dependent on its quality, as well as on water chemistry, such as pH and iron concentration (Lindell et al. 1995; Bertilsson and Tranvik 2000; Panneer Selvam et al. 2019) while other studies have found no such relationships (Cory et al. 2014). A significant share of the AQY variability between lakes can be explained by simple optical parameters (Koehler et al. 2016), allowing for estimates of photochemical DIC production when system-specific AQY spectra are not available.

In this study, we used data of such optical parameters from 70 Scandinavian lakes along a gradient of DOC concentrations, together with correlation estimates between the absorption coefficient at 420 nm (a_{420}) and the specific UV absorption coefficient at 400 nm ($SUVA_{400}$) and the AQY (Koehler et al. 2016) to estimate the lakes' wavelength specific AQY spectra. Together with atmospheric radiative modeling, we then simulated the photochemical DIC production in the study lakes. We further estimated the lakes' primary production using lake-specific phytoplankton absorption coefficients and in situ irradiance. Finally, we calculated the air-water CO_2 flux through surface water CO_2 concentrations, temperature and wind speed, using Fick's law of diffusion and Henry's law to find the CO_2 deficit from concentrations at equilibrium with the atmosphere. Assuming that the deviation of CO_2 from saturation is kept at steady state due to production, lateral input, evasion, and consumption we estimated the sum of total lake CO_2 production and the lateral input as the sum of the consumption and evasion. This allowed us to calculate the relative contribution of photochemical DIC production to lake carbon cycling. As shortwave radiation attenuates quickly in the water column of lakes, we expect all incoming photochemically reactive photons to be absorbed within the top few meters of all lakes, even the clear ones. Therefore, we hypothesized that the total amount of photomineralization of DOC would be similar in all lakes regardless of their CDOM concentrations.

Methods

Study sites

During July and August of 2011, 77 lakes along a geographical gradient between western Norway and eastern Sweden were sampled (Fig. 1). The lakes were chosen to represent gradients in DOC and total phosphorus (TP), aiming for an orthogonal gradient between these parameters, and to avoid strong temperature gradients with respect to latitude and altitude. All lakes met the following criteria: latitude 57–64°N, altitude < 600 m, surface area > 1 km^2, pH > 5, TP < 30 μg l^{-1}, and DOC < 30 mg l^{-1}.

Field sampling

Composite samples (15 L in total) were taken from 0 to 5 m in the central part of each lake during daytime, using an integrating water sampler (Hydro-BIOS, Germany). Water temperatures were measured using XRX-620 10-channel CTD (RBR Ltd., Canada). Vertical temperature profiles indicated that the thermocline was deeper than 5 m in all lakes (Fig. S1) and the integrated 0–5 m samples could be considered representative of the entire mixed layer of the lakes. Vertical profiles of scalar irradiance in the photosynthetically active radiation (PAR) region (400–700 nm; E_d) were measured using a spherical irradiance sensor (BioSpherical instruments) attached to a 10 channel CTD profiler (WRW620. RBR Ltd., Canada). The sensor was lowered at a rate of approximately 20 cm s^{-1} with a sampling rate of 6 Hz. The vertical attenuation coefficient for scalar PAR (K_dPAR) was estimated by taking the median of the distribution of slopes obtained from regressing natural log-transformed E_d against depth (z) for each 10 sampling points (i.e., sliding windows). This was done to correct for temporal changes in irradiance caused by for example wave action and clouds during the haul. pH in the samples was measured within 1 h after sampling using a handheld pH-meter (PHM201, Radiometer Analytical, France).

Laboratory analyses

Concentrations of total phosphorus (TP), total organic carbon (TOC), and total nitrogen (TN) were measured in two accredited laboratories, at the Norwegian Institute for Water Research (NIVA) and at the University of Oslo (UiO). Differences between laboratories were small for TOC and TN but slightly higher for TP. Regressions of UiO vs. NIVA measurements had the following statistics: TP: $R^2 = 0.77$, residual standard error (RSE) = 2.27 μg l^{-1}; TOC: $R^2 = 0.99$, RSE = 0.25 mg l^{-1}; TN: $R^2 = 0.91$, RSE = 81 μg l^{-1}. There were no systematic differences between the laboratories and the averages of the results were used in the subsequent analysis. DOC was calculated as the difference between the total organic carbon (TOC) and particulate organic carbon (POC). TOC was

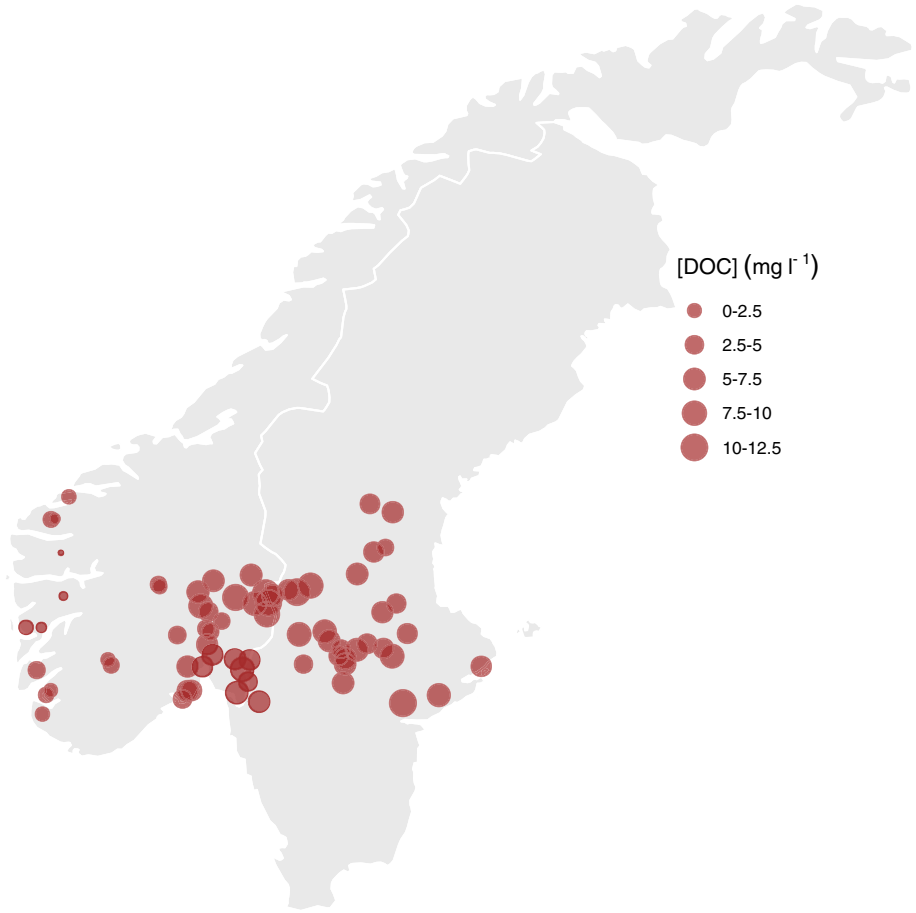

Fig. 1. Lakes included in the survey. The sizes of the symbols scale with the concentration of dissolved organic carbon (DOC; mg l^{-1}).

measured by infrared CO_2 detection after catalytic high temperature combustion (Shimadzu TOC-VWP analyzer (UiO), or Phoenix 8000 TOC-TC analyzer (NIVA)). On average, >95% of the TOC was in dissolved form (DOC). POC was measured on an elemental analyzer (Flash EA 1112 NC, Thermo Fisher Scientific, Waltham, Massachusetts) through rapid combustion in pure oxygen of a pre-combusted GF/C-filter with particulates. TP was measured on an auto-analyzer as phosphate after wet oxidation with peroxodisulfate in both laboratories. TN was measured on unfiltered samples by detecting nitrogen monoxide by chemiluminescence using a TNM-1 unit attached to the Shimadzu TOC-VWP analyzer (UiO), or detection of nitrate after wet oxidation with peroxodisulfate in a segmented flow auto-analyzer (NIVA). Concentrations of CO_2 and O_2 were determined by automated gas chromatography (GC) analysis with back-flushing H_2O (see Yang et al. 2015 for details). Total iron (Fe) was measured using an inductively coupled plasma mass spectrometer (ICP-MS, PerkinElmer NexION 300, Norwalk, Connecticut) equipped with three quadrupole mass analyzers, a cyclonic spray chamber, and a concentric nebulizer. Three subsamples from each lake were measured to evaluate the analytical precision.

For measurements of particulate absorbance spectra, water samples (150–170 mL, depending on particle load) were filtered onto 25 nm Whatman GF/C glass filters under low vacuum. The filters were placed in the entrance of an integrating sphere (ISR 2200, Shimadzu scientific instruments, Columbia, Maryland) attached to a double beam Shimadzu UV-2550 spectrophotometer, and optical density was measure for each nm from 400 to 800 nm. After the first measurement, the sample filters were bleached with sodium hypochlorite (Tassan and Ferrari 1995). The bleaching oxidizes all pigments, leaving only organic and inorganic detritus, including de-pigmented algal remains, unbleached. The optical density of this nonalgal particulate (NAP) matter was then measured and the absorption coefficients (m^{-1}) of total particulate matter and nonalgal particulate matter were calculated according to Mitchell et al. (2002), using the algorithm of Bricaud and Stramski (1990) to estimate the path-length amplification factor (β). Finally, the absorption coefficient spectra of phytoplankton pigments were calculated as the difference between the total particulate and the NAP absorption coefficient spectra. DOC absorbance spectra from 400 to 700 nm (1 nm resolution) were measured in 0.2 μm filtered water samples

(Acrodisc 0.2 μm polyethersulfone membrane syringe filter, Pall Life Sciences, Port Washington, NY) using a 50 mm quartz cuvette. Absorption coefficient spectra were calculated according to Mitchell et al. (2002). Due to missing values of some of the absorbance measurements, seven lakes had to be omitted, giving a data set of 70 lakes for further analysis.

Primary production calculations

Area-specific primary production (PP_A; mg C m^{-2} d^{-2}) was calculated using a bio-optical model based on lake-specific phytoplankton absorption coefficients, in situ irradiance, and the light dependent quantum yield of photosystem II measured by a Pulse Amplitude Modulated (PAM) fluorometer (AquaPen, PSI Czech Republic). In brief, this bio-optical model is based on estimating the in vivo rate of light absorption by phytoplankton, and subsequently electron transport rates (ETRs) through photosystem II (PSII) using information about the light-dependent quantum yield of photochemistry in PSII. ETR can further be converted to a rate of gross carbon fixation by assuming an appropriate value for the quantum yield of CO_2 fixation (Kromkamp and Forster 2003; Suggett et al. 2010). While the method could be sensitive to phytoplankton community composition related to their pigments and light capturing properties, it has gained increased interest over the last two decades because it offers a fast and inexpensive way of obtaining PP estimates (see Thrane et al. 2014 for details). A comparison of this method and empirical estimates for PP in boreal lakes demonstrates a good accordance (Thrane et al. 2014). The method is thus a feasible tool for assessment of primary production across a large number of sites. It also avoids many of the pitfalls of ^{14}C-bottle incubation, which in any case could not have been applied in this kind of synoptic, snapshot survey with sampling from a plane spanning many lakes over a large geographical area.

Wavelength-specific AQY spectrum

Koehler et al. (2016) found the strongest predictors of AQY to be the Napierian absorption coefficient at 420 nm (a_{420}; m^{-1}) and specific UV absorption coefficient at 254 nm ($SUVA_{254}$; L mg C^{-1} m^{-1}) (Kirk 1994). The data set in this study only contained optical data for wavelengths in the PAR band and therefore the relation between AQY and $SUVA_{400}$ (B. Koehler, unpublished data, 2016) (Table S2) was used instead of $SUVA_{254}$.

A linear mixed effects model with the measured AQY as the response variable, a_{420}, $SUVA_{400}$, and wavelength as fixed effects, and intercept as a random effect was run for the lakes in Koehler et al. (2016) using the lme4 package in R (Bates et al. 2014).

$$\ln(\Phi) \sim a_{420} + SUVA_{400} + \lambda + (1|lake) \quad (1)$$

Where Φ is AQY for DIC photoproduction, λ is the wavelengths in the measured wavelength region (400–700 nm in steps of 1 nm), and the (1|lake) term captures other between-lake variations not related to chromophoric DOM (CDOM) quality. The Napierian absorption coefficient at 420 nm (a_{420}) is a proxy for CDOM content, such that the higher the a_{420}, the browner the lake. We used the AQY model on data from the lakes in Koehler et al. (2016) using $SUVA_{254}$ and a_{420} and compared it to the model with $SUVA_{400}$ and a_{420}. The models resulted in close to exactly the same AQY spectra (Fig. S4) and hence we did not lose information modeling the AQY from $SUVA_{400}$ instead of $SUVA_{254}$. The model was then used to predict the AQY spectra for the 70 study lakes.

The arm package in R (Gelman et al. 2018) was used to generate Monte Carlo samples of fixed effect parameters of the linear model, which was used to propagate model uncertainties to the estimated lake specific AQYs over the entire spectrum (300–600 nm; Figs. S2 and S3). AQY spectra were extrapolated to wavelengths < 400 nm using the exponential model (Eq. 1). The irradiation model included wavelengths between 300 and 600 nm and therefore the AQY spectra were also cut at 600 nm.

Irradiation model

Daily integrated downwelling scalar irradiation spectra (300–600 nm) just below the water surface were obtained using the libRadtran model (version 1.6) for radiative transfer (Mayer and Kylling 2005), parameterized and cloud corrected as described in Koehler et al. (2014). The clear-sky spectra were integrated with calculated solar zenith angles and measurements of ozone column fields in hourly time steps at the coordinates of each lake. The true solar zenith angle was calculated with hourly time step for each lake and day for a month between early July and early August of 2011 (i.e., the time period of field sampling), using approximations in the Astronomical Almanac (Michalsky 1988). The actual ozone column fields for the same time were extracted from the archive operational runs of the Integrated Forecasting System at the European Centre for Medium-Range Weather Forecasts (http://www.ecmwf.int/research/ifsdocs/CY33r1/index.html). To correct for attenuation by clouds, total cloud cover data were retrieved for the requested time period at the lakes coordinates from the archive of the operational mesoscale analysis system at the Swedish Meteorological and Hydrological Institute (Häggmark et al. 2000).

Photochemical DIC production in the lakes

According to the photon budget approach (Kirk 1994), absorption spectra for the lakes were modeled for DOC ($a_{DOC}[\lambda]$; m^{-1}) (Twardowski et al. 2004), nonalgal particles ($a_{NAP}[\lambda]$; m^{-1}) (Shen et al. 2012), phytoplankton ($a_{PP}[\lambda]$; m^{-1}), all from lake samples and for standardized water ($a_{water}[\lambda]$; m^{-1}) (Wozniak and Dera 2007). All absorption spectra were extrapolated from the measured PAR band to 300 nm using linear mixed effect models with prediction uncertainties

propagated through Monte Carlo samples generated by the arm package in R (Gelman et al. 2018).

The total absorption coefficient spectrum ($a_{\text{total}}[\lambda]$; m^{-1}) was calculated as the sum of $a_{\text{DOC}}(\lambda)$, $a_{\text{NAP}}(\lambda)$, a_{water} (λ), and $a_{\text{PP}}(\lambda)$ (Kirk 1994) and the relative contribution of DOC to the total absorption ($k_{\text{DOC}}(\lambda)$) was calculated as the $a_{\text{DOC}}(\lambda)$ to $a_{\text{total}}(\lambda)$ quotient (Fig. S5). Finally, the wavelength-specific photon absorption by DOC per depth unit ($E_{\text{abs,p}}$ [λ, z]; mol m^{-3} d^{-1} nm^{-1}) was calculated as the depth derivative of the attenuation profile, weighted by the relative DOC contribution:

$$E_{abs,p}(\lambda, z) = E_p(\lambda) e^{-a_{total}(\lambda) z} a_{DOC}(\lambda) \quad (2)$$

where E_{p} is the photon flux ($E_{\text{p}}(\lambda)$; mol m^{-2} d^{-1} nm^{-1}) at the lake surface from the modeled irradiation spectra and z is depth (m). Solving Eq. (2) for $z \to 0$, i.e., just below the surface, the DOC absorbed photons per unit volume is given by:

$$E_{abs,p}(\lambda, 0) = E_p(\lambda) a_{DOC}(\lambda) \quad (3)$$

Boreal lakes generally absorb all incoming irradiation (Kirk 1994; Koehler et al. 2014; Thrane et al. 2014). Assuming that this also is the case for the lakes in this study, integrating Eq. (3) over the entire water column ($\int_0^\infty E_{abs,p}(\lambda, z) dz$), DOC absorbed photons per unit surface area ($E_{\text{abs,p}}$ (λ); mol m^{-2} d^{-1} nm^{-1}) is given by:

$$E_{abs,p}(\lambda) = E_p(\lambda) k_{DOC}(\lambda) \quad (4)$$

Wavelength-specific photochemical DIC production could then be calculated as either volumetric rates at the surface ($\psi_{\text{DIC}}[\lambda, 0]$; mol m^{-3} d^{-2} nm^{-1}) or as production rates per unit area ($\psi_{\text{DIC}}(\lambda)$; mol m^{-2} d^{-2} nm^{-1}), multiplying the photon absorption by DOC by the AQY (Φ):

$$\psi_{DIC}(\lambda, z) = E_{abs,p}(\lambda, z) \Phi_{DIC}(\lambda) \quad (5)$$

CO_2 flux

Air-water flux of CO_2 (F_{CO2}; mmol m^{-2} d^{-1}) was calculated from the surface CO_2 concentrations in each lake using Fick's law of diffusion:

$$F_{CO2} = k_{CO2} \Delta_{CO2} \quad (6)$$

where k_{CO2} (m d^{-1}) is the CO_2 gas exchange coefficient at a given temperature and Δ_{CO2} (mmol m^{-3}) is the CO_2 deficit from concentrations at equilibrium with the atmosphere, obtained using Henry's law. k_{CO2} was estimated for each lake using the gas transfer velocity (cm h^{-1}) for a gas-temperature combination with a Schmidt number of 600 (k_{600}; CO_2 at 20°C) according to Jähne et al. (1987):

$$k_{CO2} = k_{600} \left(\frac{Sc_{CO2}}{600} \right)^{-x} \quad (7)$$

where x = 2/3 if wind speed ≤ 3 ms^{-1} and x = 0.5 if wind speed > 3 ms^{-1}, Sc is the temperature dependent Schmidt number for CO_2 (Wanninkhof 1992). k_{600} is estimated from the wind speed according to Cole and Caraco (1998):

$$k_{600} = 2.07 + 0.215\, U_{10}^{1.7} \quad (8)$$

Hourly wind speed data at 10 m above ground (U_{10} in Eq. 9) at all 70 lakes were received from the Norwegian Reanalysis Archive (Furevik and Haakenstad 2012) and aggregated into July–August means.

Lake pelagic CO_2 production

From the dataset, it was not possible to distinguish between lateral input of CO_2 (surface- and ground water flow) and in-lake production of CO_2 (microbial and photochemical mineralization of DOC). Lake pelagic CO_2 production ($CO_{2,\text{prod}}$; mg C m^{-2} d^{-1}) will therefore be used as a term for the sum of the in situ DOC mineralization and the lateral input. Assuming that the deviation of CO_2 from saturation is kept at steady state due to production, lateral input, consumption and evasion, the air-water flux of CO_2 (F_{CO2}; mg C m^{-2} d^{-1}) can be written as:

$$F_{CO2} = CO_{2,prod} - PP_A \quad (9)$$

Positive and negative values of F_{CO2} are evasion and invasion across the air–water interface, respectively. Rearranging Eq. (9), we estimate $CO_{2,\text{prod}}$ as the sum of F_{CO2} and PP_{A}.

Statistical analysis

All data analysis was performed using the open-source software R version 3.4.1 (R Development Core Team, 2017). For linear modeling of the CO_2 production, consumption, and evasion in the lakes the explanatory variables were DOC (mg l^{-1}), TP (µg l^{-1}) and TN (mg l^{-1}). The predictors were chosen using AICc in backwards stepwise regression. For estimation of the best predictor, the largest value of the standardized regression coefficients was used. All error estimates are given in standard errors (standard deviation divided by the square root of the number of observations: $SE = SD/\sqrt{n}$).

Results

Modeling the AQY spectra

The optical parameters a_{420} and $SUVA_{400}$ explained 26–64% of the variation in AQY across lakes. The variation in AQY explained by the parameters decreased with wavelength giving a higher percentage explained at shorter wavelengths where AQY variability between lakes is larger (Table S2; data from Koehler et al. (2016)). The relative magnitude of the

sums of squares (SS) of the fixed terms in the model (Eq. 1) can be used to rank their contribution to the variance of the predicted AQY. While wavelength was by far the largest variance contribution (SS = 48.9; $p << 0.001$), a_{420} contributed about five times (SS = 0.87; p = 0.023) as much to the variance in modeled AQY as $SUVA_{400}$ (SS = 0.18; p = 0.027). Monte Carlo simulations of the AQY spectra based on these regression relationships (n = 70) resulted in a SE ranging between 0.9% and 1.8% of the wavelength integrated AQY's. The SE was negatively related to a_{420} (r = –0.73; data not shown), indicating that the model fits brown lakes somewhat better than clear ones. The SE of the AQY had an almost one to one fit with the SE of the DIC photoproduction. The uncertainty of the modeled AQY thus propagated through to the DIC photoproduction estimate and the uncertainties of the absorption spectra or the downwelling irradiation did not contribute substantially.

CO_2 saturation

Out of the 70 lakes in this study, 62 were supersaturated with CO_2 while 6 lakes were close to saturation or slightly undersaturated and 2 were clearly undersaturated with CO_2. DOC concentrations were strongly related to a_{420} (r = 0.88), and the CO_2 saturation deficit was positively related to both DOC and a_{420} (r = 0.50 and 0.61 for DOC and a_{420}, respectively). The CO_2 and O_2 saturation deficits were negatively correlated (r = –0.70), and the O_2 saturation deficit was negatively related to DOC concentrations and a_{420} (r = –0.74 and –0.69, respectively; Fig. S6).

Photochemical DIC production

a_{420} and $SUVA_{400}$ in the sampled lakes varied between 0.60 and 11.47 m^{-1}, and 0.16 and 1.33 L mg C^{-1} m^{-1}, respectively (Table S1). Integrating the estimated areal photochemical production of DIC (Fig. 2a), over wavelengths (300–600 nm) gave a range in photoproduced DIC between 8.4 mg C m^{-2} d^{-1} ± 1.5% and 21.4 mg C m^{-2} d^{-1} ± 1.0%; Table S1) in the lakes. Both $SUVA_{400}$ and a_{420} were negatively related to pH (r = –0.51 and r = –0.28, respectively; Fig. S7) and positively related to iron concentrations (Fe; r = 0.35 and r = 0.74 for $SUVA_{400}$ and a_{420} respectively; Fig. S7). A multiple linear regression model showed equal sized but opposite effects of pH and Fe concentrations on the estimated DIC photoproduction rates (R^2 = 0.31, Table S3). The interaction term between the predictor variables was nonsignificant (p > 0.05, Table S3).

In lakes with high a_{420}, the shorter wavelengths are absorbed at the surface, resulting in high DIC photoproduction in the top layer compared to lakes with lower a_{420} (Fig. 2b). While in the brownest lakes irradiance of all photochemically active wavelengths was absorbed within the first meter, this irradiance penetrated further in clearer lakes, allowing for DIC photoproduction to take place at greater depth. Most DIC photoproduction is induced by absorption of photons with wavelengths in the UV and violet part of the spectrum (Vähätalo et al. 2000). Of the estimated areal photochemical DIC production in all lakes 85% ± 0.1% and 93% ±

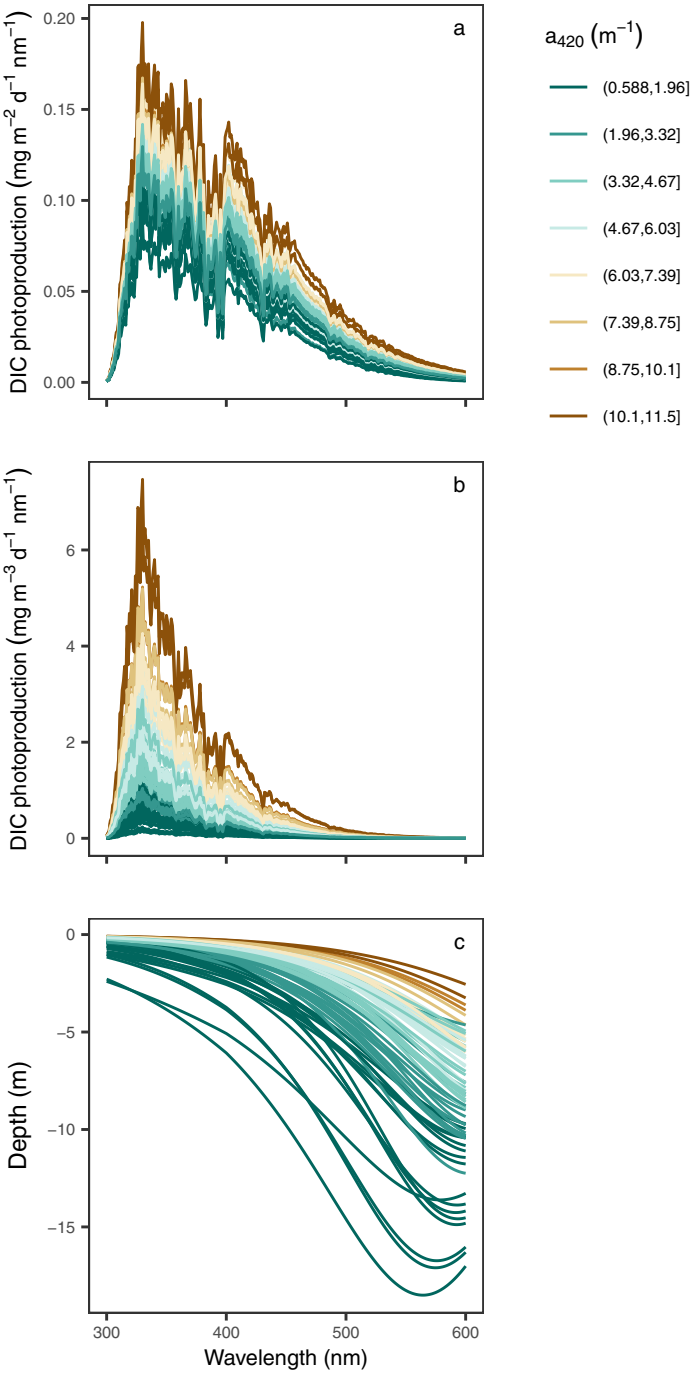

Fig. 2. Estimated photoproduction spectra of dissolved inorganic carbon (DIC) from all 70 study lakes. In **(a)**, the estimated areal DIC photoproduction (mg C m^{-2} d^{-1} nm^{-1}) spectra are shown; and **(b)** shows the estimated volumetric DIC photoproduction (mg C m^{-3} d^{-1} nm^{-1}) spectra just below the surface. In **(c)** the depth at which the volumetric DIC photoproduction (mg C m^{-3} d^{-1} nm^{-1}) is 1% of that just below the surface is shown, indicating also the depth that receives 1% of incoming radiation. The color gradient goes from dark blue for lakes with low a_{420} to brown for lakes with high a_{420}.

Table 1. Regression coefficients for regressions predicting lake pelagic CO_2 production, consumption, and evasion.

Response	Predictors	Coefficient estimates (SE, significance levels)	R^2
Lake pelagic CO_2 production	TP + TN	29.9 (±6.6***), 338.0 (±116.9**)	0.47
Areal primary production (PP_A)	DOC + TP + TN	−29.2 (±7.4***), 21.9 (±4.6***), 174.8 (±75.7*)	0.47
CO_2 flux	DOC + TP	35.4 (±8.9***), 11.2 (±4.9*)	0.33

Significance codes:
***$p < 0.001$,
**$p < 0.01$,
*$p < 0.05$.

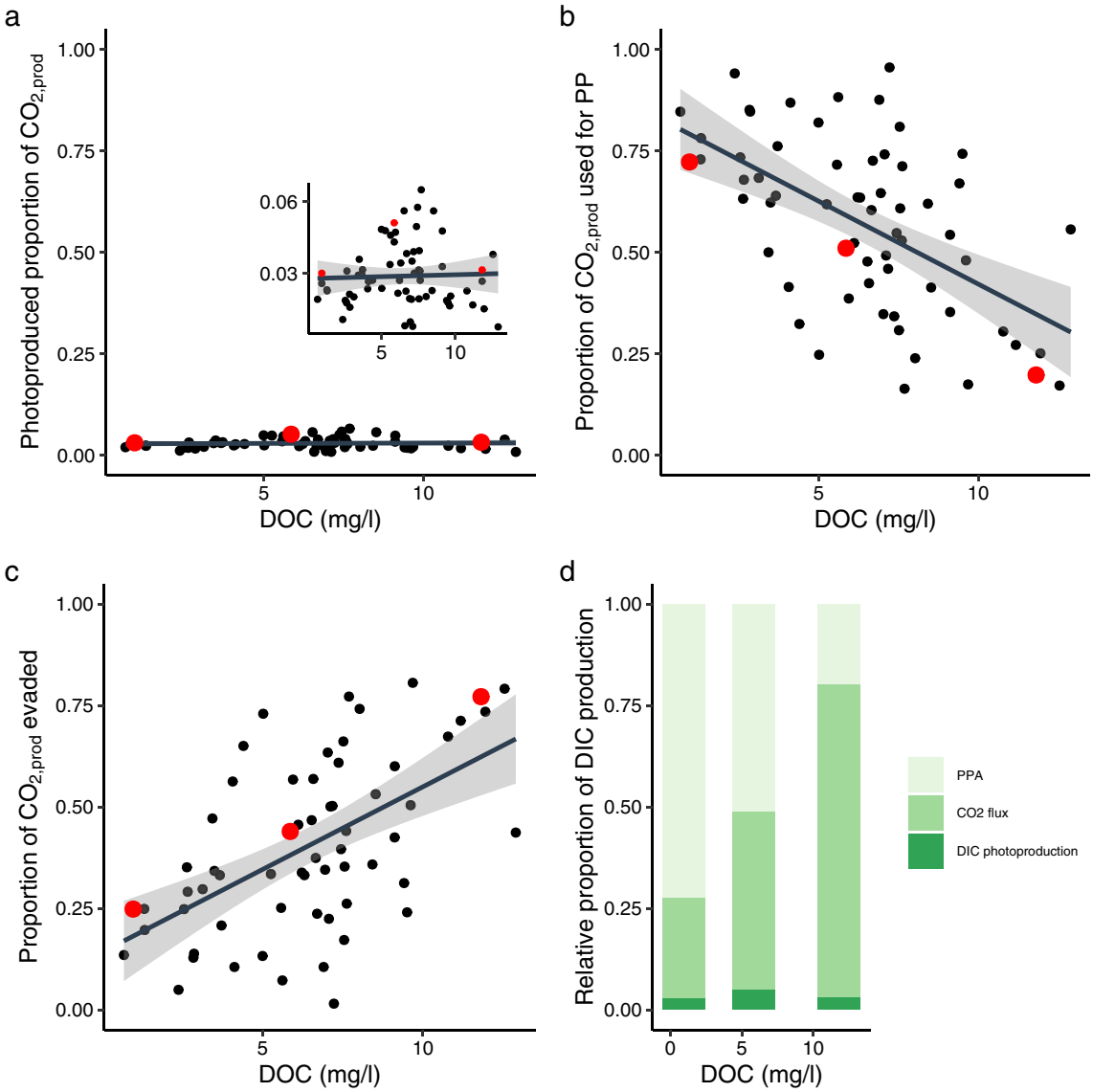

Fig. 3. The relative proportions of **(a)** DIC photoproduction (the inset figure is zoomed in on the *y*-axis); **(b)** CO_2 flux and; **(c)** areal primary production (PP_A) to total lake pelagic CO_2 production ($CO_{2,prod} = F_{CO2} + PP_A$; Eq. 9). In **(d)** is an example of the relative proportion of DIC production for three lakes with low (0.95 mg C l^{-1}), medium (5.85 mg C l^{-1}), and high (11.84 mg C l^{-1}) DOC concentrations. Red dots in the regression plots indicate the three example lakes.

0.1% was induced by wavelengths shorter than 465 and 500 nm, respectively (Fig. S5). Therefore, almost all DIC photoproduction took place in the top 5 m of all lakes, regardless of their color (Fig. 2c). In some of the clearest lakes, light of wavelengths > 500 nm penetrated as deep as 15–20 m (Fig. 2c). The contribution to total DOC photomineralization by wavelengths > 500 nm was minor (Figs. 2a and S3), and the majority of DIC photoproduction thus occurred in the top 5 m of the water column, even in the clearest lakes. The estimated percentage of the DOC standing stock that was photomineralized each day averaged about 2% (0.2–3%) at the surface and 0.3% (0.1–1%) at 1-m depth (Fig. S8). At the surface, the photomineralized share of the standing stock of DOC increased somewhat with increased DOC concentration, while at one meter the relationship was the opposite.

Lake pelagic CO_2 production and consumption

Estimations of summer lake pelagic CO_2 production (photochemical and biological mineralization + lateral input of CO_2) in the studied lakes ranged between 120 and 1770 mg C m^{-2} d^{-1}. The best predictors for lake pelagic CO_2 production were TP (μg P l^{-1}) and TN (mg N l^{-1}; Table 1). The relative contribution of DIC photoproduction to lake pelagic CO_2 production averaged 3.0% ± 0.2% regardless of DOC concentration (Fig. 3a,d). Primary production in the lakes was negatively related to DOC concentration and positively related to nutrient content, mainly TP (Table 1). The share of lake pelagic CO_2 production used for primary production was thus smaller in lakes with a high DOC concentration than in lakes with a low DOC concentration (Fig. 3b,d).

CO_2 flux

The majority of the lakes were net sources of CO_2 to the atmosphere. The CO_2 flux ranged from –0.12 to 1.0 g C m^{-2} d^{-1}. CO_2 evasion from lakes was best explained by DOC concentration, followed by TP (Table 1). Assuming that all photochemically produced DIC was emitted as CO_2 from supersaturated lakes, the relative contribution of estimated DIC photoproduction to total CO_2 efflux ranged between 1.4% and 36%, averaging 9% ± 1%, and with higher contribution in lakes with low than in lakes with high DOC concentrations (Fig. S7). The source of the remaining CO_2 efflux must be attributed to respiration and lateral CO_2 input. Of the total DIC production in the lakes, a larger share was emitted as CO_2 in lakes with high than in lakes with low DOC concentrations (Fig. 3c,d).

Discussion

We estimated DIC photoproduction in boreal lakes using modeled spectra of irradiance and AQY, and spectra of attenuation coefficients and absorption extrapolated from the measured PAR to the UV region from 70 lakes in Norway and Sweden. We found that DIC photoproduction contributed on average 9% ± 1% to the CO_2 emission from the lakes. Regarding that this percentage decreases with increased DOC concentrations and that water temperatures as well as DOC and nutrient concentrations in boreal lakes are increasing (Larsen et al. 2011*b*; O'Reilly et al. 2015), we expect that the relative contribution of sunlight for CO_2 production in boreal lakes may decline in the future.

The AQY spectra were modeled using regressions between AQY at discrete wavelengths and the optical parameters $SUVA_{400}$ and a_{420}, which were set up based on AQY spectral measurements of 25 lakes worldwide (Koehler et al. 2016). While a_{420} is a proxy for CDOM content, $SUVA_{400}$ is well correlated with DOC aromaticity, and both parameters describe absorbing properties of the DOC. (Koehler et al. 2016). Even though $SUVA_{400}$ is well correlated with DOC aromaticity, $SUVA_{254}$ is usually a better indication of DOC aromaticity. Likewise, in the study by Koehler et al. (2016), $SUVA_{254}$ was somewhat better correlated with AQY than $SUVA_{400}$ was. However, the difference in R^2 between $SUVA_{400}$ and $SUVA_{254}$ as linear predictors of AQY was minor (Table S2). Running the AQY model (Eq. 1) on the data from Koehler et al. (2016) with $SUVA_{254}$ produced similar spectra as with $SUVA_{400}$, mean values of the Monte Carlo simulations had a one to one fit (Fig. S4) and there were no significant differences in SEs between the two. We therefore used the measured $SUVA_{400}$ instead of an extrapolated value of $SUVA_{254}$. The uncertainty in the modeled AQY spectra propagated through to the DIC photoproduction estimates. The SEs in the modeled AQY's were however small (1.2% ± 0.02%) and the errors in the estimated DIC photoproduction were therefore also small. Additionally, the AQY spectra estimated in this study match spectra from other studies on boreal lakes well (Koehler et al. 2014; Groeneveld et al. 2016; Vachon et al. 2016).

Estimated DIC photoproduction contributed about 3% (1–5%) of the total production and lateral inflow of CO_2 in the 62 lakes supersaturated with CO_2. Further, assuming that all photochemically produced of DIC is outgassed from the lakes, the relative share of DIC photoproduction to total CO_2 emission averaged about 9% across the 70 study lakes. These results conform to earlier studies on photomineralization of DOC and CO_2 flux from boreal lakes. For example, the contribution of DIC photoproduction to total DOC mineralization in two Swedish humic lakes amounted to about 7% (Jonsson et al. 2001) and 6% (Chmiel et al. 2016). In a third lake, the mean contribution of DIC photoproduction to CO_2 out flux was 1–8%, depending on the time of the year (Groeneveld et al. 2016). Or, in a large-scale modeling study for 1086 Swedish lakes, the mean contribution of DIC photoproduction to out flux of CO_2 was about 12% and upscaling to the entire boreal region about 9–12% (Koehler et al. 2014). However, in other aquatic systems than boreal lakes, photochemical degradation has been found to have an important role in aquatic carbon cycling. In arctic surface waters photochemical reactions accounted for 75% of the total DOC processed (Cory et al. 2014) and in a number of boreal streams photochemical

degradation accounted for more than 60% of DOC losses (Molot and Dillon 1997).

Rates of DIC photoproduction in lakes are controlled by three wavelength-dependent processes: the amount of sunlight reaching the lake surface; the fraction of this that is absorbed by CDOM across wavelengths; and the amount of DIC produced per unit absorbed light (AQY) (Cory and Kling 2018). The latter two processes had the largest variations between our 70 study lakes while the solar irradiation spectra were similar, owing to the fact that we sampled in a similar geographic region and time, and that cloud cover variability was low. Both AQY and the CDOM fraction of absorbed irradiance are dependent on the quantity and quality of CDOM in the water. Volumetric DIC photoproduction rates at specific depths are therefore closely related to CDOM content.

While the variability in absorption coefficients between lakes was substantial, the total estimated areal photochemical production of DIC did not differ as much, as similarly shown in earlier studies (Granéli et al. 1996; Koehler et al. 2014). Lower a_{420} allows light to penetrate deeper down in the water column and DIC photoproduction to take place at greater depths compared to waters with higher a_{420}. In the latter, all short wavelength photons are strongly absorbed by the DOC and therefore all photoproduction occurs close to the water surface. The absolute areal DIC photoproduction rates were similar whether they were integrated over the entire lake depth or over five meters, indicating that even in the clearest lakes all photochemical production of DIC takes place in the top five meters, where the sampling took place. Both $SUVA_{400}$ and a_{420} were negatively related to pH, and positively related to Fe concentrations (Fig. S9). This implies that the effect of extrinsic variables may affect the intrinsic properties of the DOC and therefore the DIC photoproduction rates. A positive correlation between Fe concentrations and CDOM absorption (e.g., a_{420}) has been shown before (Kritzberg and Ekström 2011). $SUVA_{400}$ was principally related to pH. As $SUVA_{400}$ is a measure of the aromatic character of the DOC, this implies that aromaticity is increasing at decreasing pH. In acidic waters, DIC photoproduction rates have frequently been reported to increase with decreasing pH (Panneer Selvam et al. 2019). In alkaline waters, the relationship between photochemical degradation of DOC and pH is less certain. While some studies find photomineralization rates to keep decreasing as pH increases (Bertilsson and Tranvik 2000; Molot et al. 2005), others report that they start increasing as pH increases above 7 (Pace et al. 2012; Panneer Selvam et al. 2019). Iron concentrations are also known to interact with pH, having a stronger positive effect on CDOM absorption and hence DIC photoproduction rate under acidic conditions (Gu et al. 2017). However, the pH in the study lakes ranged between 6.3 and 8.0 with two outliers at 5.4 and 8.9 and was thus close to neutral, possibly explaining why the interaction term between Fe and pH in our model was not significant.

Photons entering the water column are likely to be absorbed, if not by DOC, by phytoplankton, nonalgal particles, or by the water itself. Lake absorption spectra show that close to all the photons in the UV region and the largest fraction of the photons in the PAR region were absorbed by DOM, and only a small number were absorbed by other chromophoric compounds (Fig. S3; see also Thrane et al. (2014)). In this study, absorption spectra were only measured in the PAR region. Since the major part of absorption by DOC and thereby the major part of photochemical mineralization of DOC takes place in the UV region, we extrapolated the absorption spectra to wavelengths < 400 nm. We acknowledge that the extrapolation may have led to increased uncertainties of the absorption estimates and through that to increased uncertainties of the DIC photoproduction estimates. However, DOC absorption is rather well studied and the spectra are known to be approximately exponential (Bricaud et al. 1981). Therefore, the mean value of the Monte Carlo simulated spectra and their SE can be assumed to capture most of the uncertainty of the absorption and its propagation through to the DIC photoproduction estimates. For wavelengths between 280 and 400 nm, the DOC absorption fraction in boreal lakes is generally close to 1, and the DOC concentrations are often sufficient for absorption of all incoming photons in this waveband in the top meters of the water column (Williamson et al. 1996). In lakes with high a_{420}, primary production is constrained to the surface layer due to high light attenuation, resulting in lower rates of primary production on the whole-lake scale (Thrane et al. 2014). However, in regard to the areal photochemical DIC production, the critical limitation is the total amount of DOM-absorbed photons regardless of where in the water column they are absorbed. The major part of the estimated photoproduction of DIC took place above 5 m (Fig. 2c) and was therefore within the mixed zone of the lakes (Fig. S1). The photic zone is deeper in clear than in brown lakes and we can expect that some DIC photoproduction might take place below the mixed zone. However, the photons reaching depths deeper than 5 m are of longer, less photoreactive wavelengths and the contribution of DIC photoproduction at such depth to total lake DIC photoproduction is minor.

While some studies have reported that the vast majority of the CO_2 evasion from boreal lake surfaces is explained by pelagic respiration (Jonsson et al. 2001), others have shown that input of DIC has a larger role than previously thought (Weyhenmeyer et al. 2015). In this study, it was not possible to distinguish between lateral flow and respiration; lake pelagic CO_2 production is therefore used as a common term for the sum of the two. There was, however, a strong relationship between O_2 and CO_2 saturation deficits ($r = -0.70$; Fig. 4). The intercept was not significantly different from 0, meaning that lakes that were saturated with O_2 were also saturated with CO_2. This relationship indicates that microbial respiration was the predominant source of CO_2 in the lakes. Furthermore, both O_2 and CO_2 concentrations correlated well with DOC,

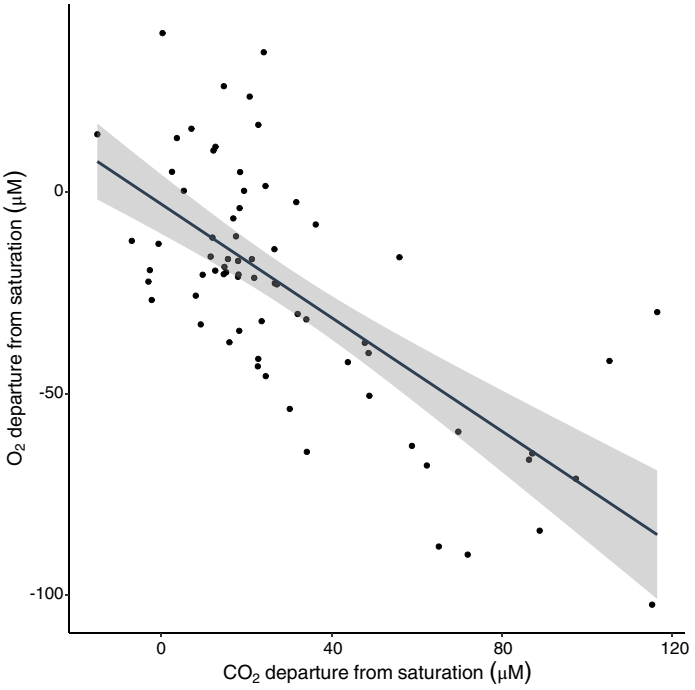

Fig. 4. Lake O_2 departure from saturation with the atmosphere vs. CO_2 departure from saturation with the atmosphere ($y = -0.70x - 3.02$, $R^2 = 0.49$, $p << 0.001$).

but not with chlorophyll *a* (Fig. S10). This suggests that the major DOC source for microbial degradation was of terrestrial origin. The strong relationship between DOC concentrations and a_{420} confirms that the dominant part of the DOC pool in the lakes originated from the terrestrial surroundings.

Sampling of the lakes used in this study was performed during mid-summer in July and August. Our results cannot be extrapolated to estimate annual rates, but rather present a picture of summer conditions. Photochemical reactivity of DOC depends on the degree of aromaticity (Bertilsson and Tranvik 2000). As DOC leaves the soil and enters the aquatic systems, it will be altered through both biological and photochemical reactions and lose aromaticity (Brinkmann et al. 2003), becoming less photoreactive. Hence, the DOC photochemical reactivity is linked to light exposure time. AQY spectra of photochemical DOC mineralization show pronounced seasonal variability. Photomineralization rates were found to be higher during seasons with high inputs of DOC to lakes, after snowmelt during spring flood (Vachon et al. 2016), and in connection to rain events in autumn, and lower in summer when DOC inputs are low (Groeneveld et al. 2016; Vachon et al. 2016). Photochemical DIC production is dependent on both irradiation and on DOC composition. The AQY might thus be higher in autumn than in summer but due to less sunlight in autumn than in summer, the amount of DIC photoproduction does not necessarily differ substantially between the two seasons. However, increased light absorption due to brownification may lead to enhanced lake stratification (Williamson et al. 2015), and especially it may give rise to microlayers of stratification at the surface where most irradiance is absorbed. The CO_2 concentrations in these microlayers could thus be much higher than in the underlying water, causing increased rates of photochemically induced CO_2 emissions from brown lakes, especially during the summer months when daily irradiation rates are high. We did not see any indication of increased thermal stratification with increased CDOM content in the study lakes. The CO_2 concentrations of the composite samples can therefore be assumed to represent the concentrations in the entire mixed layers.

On the other hand, pelagic respiration is strongly related to temperature and, therefore, also has a seasonal pattern with higher rates during summer than the rest of the year (Vachon et al. 2016). The relative contribution of photomineralization to total pelagic CO_2 production can thus be assumed to be lower during summer. This was confirmed by Vachon et al. (2016) where the relative contribution of photochemical DIC production to total pelagic CO_2 production in three lakes averaged 14% over the year with larger contribution in spring (26%) than in summer (7.6%) and autumn (12%). The mean value of lake pelagic CO_2 production in the 70 lakes in our study was 616.4 mg C m^{-2} d^{-1}, ranging from 118.7 to 1769.1 mg C m^{-2} d^{-1}. These numbers accord with measurements of DOC mineralization in other boreal lakes at summer conditions (Jonsson et al. 2001; Vachon et al. 2016). The DIC photoproduction rates and their relative contribution to lake CO_2 production and evasion also correspond to measures and estimates in previous studies (Jonsson et al. 2001, Vachon et al. 2016). The typical seasonal variations in both microbial and photochemical mineralization rates reported from other lakes make it likely that the role of DIC photoproduction also in the 70 boreal lakes of this study is larger during spring and autumn conditions than found here at summer conditions.

In this study, we estimated photochemical mineralization of DOC. Other photochemical processes in the water column may also have a large impact on the aquatic carbon cycle. Such processes are photomineralization of organic nutrients and partial photooxidation of DOC (Bertilsson and Tranvik 2000). In the latter processes, recalcitrant DOC is transformed to more biologically available organic compounds (Bertilsson and Tranvik 1998). Microbial consumption of such photodegraded compounds is thus often preferred over the nonphotodegraded compounds (Allesson et al. 2016). Although most photochemical processes take place near the surface, photochemically produced carboxylic acids may mix downwards and be a source of labile DOC in the entire mixed layer (Bertilsson and Tranvik 1998). Enhanced microbial degradation of photodegraded DOC may have an impact on aquatic carbon cycling as large as photomineralization.

Post-acidification recovery, increased vegetation cover in catchments, and a wetter climate promote carbon export to

lakes (Finstad et al. 2017; de Wit et al. 2018). Concentrations of allochthonous DOC are thus predicted to increase in most boreal lakes (Larsen et al. 2011*b*). Input of DOC in boreal lakes is correlated with export of TP and TN (Dillon and Molot 2005), and the predicted increased nutrient levels will most likely promote microbial activity and thus pelagic CO_2 production. Although DOC and TP have contrasting effects on primary production, the net effect of enhanced levels will probably be a reduced primary production due to light attenuation in most lakes with initial moderate to high DOC concentrations (Thrane et al. 2014). In lakes with low initial levels of DOC, an increase in DOC and nutrient levels could lead to enhanced primary production, and thus an enhanced level of autochthonous DOC which in turn could result in enhanced microbial respiration (Lapierre and del Giorgio 2014). Increased DOC input will thus most likely lead to enhanced levels of heterotrophy in boreal lakes (Larsen et al. 2011*a*). Moreover, higher levels and more frequent input of fresh, photolabile, DOC are to be expected and therefore the AQY and by that DIC photoproduction can be expected to increase as well. However, the rather small difference in estimated areal DIC photoproduction between lakes compared to the wide ranges in DOC and a_{420} indicates that enhanced rates of photochemical mineralization will not be a major contributor to shifting levels of boreal lake net heterotrophy. In all lakes, all photons active to DOC photochemistry were absorbed within the top five meters, regardless of DOC concentration. This suggests that the contribution of enhanced rates of DIC photoproduction to lake net heterotrophy will probably be largest when clear, shallow lakes undergo browning. While the observed strong increase in surface water temperatures (O'Reilly et al. 2015) will promote microbial respiratory activity, photomineralization is only weakly temperature dependent (Chatwal and Arora 2007), hence the relative contribution of DIC photoproduction to total CO_2 production will most likely decrease in boreal lakes under a changing climate.

References

Allesson, L., L. Ström, and M. Berggren. 2016. Impact of photochemical processing of DOC on the bacterioplankton respiratory quotient in aquatic ecosystems. Geophys. Res. Lett. **43**: 7538–7545.

Bates, D., Mächler, M., Bolker, B. & Walker, S. 2014. Fitting linear mixed-effects models using lme4. **67**: 1–48.

Bertilsson, S., and L. J. Tranvik. 1998. Photochemically produced carboxylic acids as substrates for freshwater bacterioplankton. Limnol. Oceanogr. **43**: 885–895.

Bertilsson, S., and L. J. Tranvik. 2000. Photochemical transformation of dissolved organic matter in lakes. Limnol. Oceanogr. **45**: 753–762.

Bricaud, A., A. Morel, and L. Prieur. 1981. Absorption by dissolved organic matter of the sea (yellow substance) in the UV and visible domains 1. Limnol. Oceanogr. **26**: 43–53.

Bricaud, A., and D. Stramski. 1990. Spectral absorption coefficients of living phytoplankton and nonalgal biogenous matter: A comparison between the Peru upwelling areaand the Sargasso Sea. Limnol. Oceanogr. **35**: 562–582.

Brinkmann, T., D. Sartorius, and F. H. Frimmel. 2003. Photobleaching of humic rich dissolved organic matter. Aquat. Sci. **65**: 415–424.

Chatwal, G. R., and M. Arora. 2007. Organic photochemistry. Himalaya Publishing House. Mumbay, India.

Chmiel, H. E., et al. 2016. The role of sediments in the carbon budget of a small boreal lake. Limnol. Oceanogr., **61**, 1814–1825.

Cole, J. J., and N. F. Caraco. 1998. Atmospheric exchange of carbon dioxide in a low-wind oligotrophic lake measured by the addition of SF6. Limnol. Oceanogr. **43**: 647–656.

Cole, J. J., M. L. Pace, S. R. Carpenter, and J. F. Kitchell. 2000. Persistence of net heterotrophy in lakes during nutrient addition and food web manipulations. Limnol. Oceanogr. **45**: 1718–1730.

Cole, J. J., and others. 2007. Plumbing the global carbon cycle: Integrating inland waters into the terrestrial carbon budget. Ecosystems, **10**, 172–185.

Cory, R. M., and G. W. Kling. 2018. Interactions between sunlight and microorganisms influence dissolved organic matter degradation along the aquatic continuum. Limnol. Oceanogr. Lett. **3**: 102–116.

Cory, R. M., C. P. Ward, B. C. Crump, and G. W. Kling. 2014. Sunlight controls water column processing of carbon in arctic fresh waters. Science **345**: 925–928.

de Wit, H. A., R.-M. Couture, L. Jackson-Blake, M. N. Futter, S. Valinia, K. Austnes, J.-L. Guerrero, and Y. Lin. 2018. Pipes or chimneys? For carbon cycling in small boreal lakes, precipitation matters most. Limnol. Oceanogr. Lett. **3**: 275–284.

Dillon, P. J., and L. A. Molot. 2005. Long-term trends in catchment export and lake retention of dissolved organic carbon, dissolved organic nitrogen, total iron, and total phosphorus: The Dorset, Ontario, study, 1978–1998. J. Geophys. Res. Biogeo. **110**.

Finstad, A. G., E. B. Nilsen, D. K. Hendrichsen, and N. M. Schmidt. 2017. Catchment vegetation and temperature mediating trophic interactions and production in plankton communities. PLOS One **12**: e0174904.

Furevik, B. R., and H. Haakenstad. 2012. Near-surface marine wind profiles from rawinsonde and NORA10 hindcast. J. Geophys. Res. Atmos. **117**.

Gelman, A., et al. 2018. Package 'arm'.

Granéli, W., M. Lindell, and L. Tranvik. 1996. Photo-oxidative production of dissolved inorganic carbon in lakes of different humic content. Limnol. Oceanogr. **41**: 698–706.

Groeneveld, M., L. Tranvik, S. Natchimuthu, and B. Koehler. 2016. Photochemical mineralisation in a boreal brown water lake: Considerable temporal variability and minor contribution to carbon dioxide production. Biogeosciences **13**: 3931–3943.

Gu, Y., A. Lensu, S. Perämäki, A. Ojala, and A. V. Vähätalo. 2017. Iron and pH regulating the photochemical mineralization of dissolved organic carbon. ACS Omega **2**: 1905–1914.

Häggmark, L., K.-I. Ivarsson, S. Gollvik, and P.-O. Olofsson. 2000. Mesan, an operational mesoscale analysis system. Tellus A Dynam. Meteorol. Oceanogr. **52**: 2–20.

Hessen, D. O. 1992. Dissolved organic carbon in a humic lake: Effects on bacterial production and respiration. Hydrobiologia **229**: 115–123.

Hessen, D. O., and L. J. Tranvik. 1998. Aquatic humic substances: Ecology and biogeochemistry. Springer Science & Business Media. Berlin Heidelberg: Springer.

Jähne, B., K. O. Münnich, R. Bösinger, A. Dutzi, W. Huber, and P. Libner. 1987. On the parameters influencing air-water gas exchange. J. Geophys. Res. Oceans **92**: 1937–1949.

Jonsson, A., M. Meili, A.-K. Bergström, and M. Jansson. 2001. Whole-lake mineralization of allochthonous and autochthonous organic carbon in a large humic lake (örträsket, N. Sweden). Limnol. Oceanogr. **46**: 1691–1700.

Karlsson, J., P. Byström, J. Ask, P. Ask, L. Persson, and M. Jansson. 2009. Light limitation of nutrient-poor lake ecosystems. Nature **460**: 506–509.

Kirk, J. T. O. 1994. Light and photosynthesis in aquatic ecosystems. Cambridge, England: Cambridge Univ. Press.

Koehler, B., E. Broman, and L. J. Tranvik. 2016. Apparent quantum yield of photochemical dissolved organic carbon mineralization in lakes. Limnol. Oceanogr. **61**: 2207–2221.

Koehler, B., T. Landelius, G. A. Weyhenmeyer, N. Machida, and L. J. Tranvik. 2014. Sunlight-induced carbon dioxide emissions from inland waters. Global Biogeochem. Cycles **28**: 696–711.

Kritzberg, E., and S. Ekström. 2011. Increasing iron concentrations in surface waters—A factor behind brownification? Biogeosciences Discussions **8**: 12285–12316.

Kromkamp, J. C., and R. M. Forster. 2003. The use of variable fluorescence measurements in aquatic ecosystems: Differences between multiple and single turnover measuring protocols and suggested terminology. Eur. J. Phycol. **38**: 103–112.

Lapierre, J. F., and P. A. del Giorgio. 2014. Partial coupling and differential regulation of biologically and photochemically labile dissolved organic carbon across boreal aquatic networks. Biogeosciences **11**: 5969–5985.

Larsen, S., T. Andersen, and D. hessen. 2011*a*. The pCO2 in boreal lakes: Organic carbon as a universal predictor? Global Biogeochem. Cycle **25**.

Larsen, S., T. Andersen, and D. O. Hessen. 2011*b*. Climate change predicted to cause severe increase of organic carbon in lakes. Glob. Chang. Biol. **17**: 1186–1192.

Lindell, M. J., W. Granéli, and L. J. Tranvik. 1995. Enhanced bacterial growth in response to photochemical transformation of dissolved organic matter. Limnol. Oceanogr. **40**: 195–199.

Mayer, B., and A. Kylling. 2005. Technical note: The libRadtran software package for radiative transfer calculations—Description and examples of use. Atmos. Chem. Phys. **5**: 1855–1877.

Michalsky, J. 1988. The astronomical Almanac's algorithm for approximate solar position (1950–2050). Solar Energy **40**: 227–235.

Miller, W. L., M. Moran, W. M. Sheldon, R. G. Zepp, and S. Opsahl. 2002. Determination of apparent quantum yield spectra for the formation of biologically labile photoproducts. Limnol. Oceanogr. **47**: 343–352.

Mitchell, B., Kahru, M., Wieland, J. & Stramska, M. 2002. Determination of spectral absorption coefficients of particles, dissolved material and phytoplankton for discrete water samples. Ocean Opt. Protoc. Satell. Ocean Color Sens. Valid. Revis. **3**: 231–257.

Molot, L., and P. Dillon. 1997. Photolytic regulation of dissolved organic carbon in northern lakes. Global Biogeochem. Cycle **11**: 357–365.

Molot, L. A., J. J. Hudson, P. J. Dillon, and S. A. Miller. 2005. Effect of pH on photo-oxidation of dissolved organic carbon by hydroxyl radicals in a coloured, softwater stream. Aquat. Sci. **67**: 189–195.

O'Reilly, C. M., and others. 2015. Rapid and highly variable warming of lake surface waters around the globe. Geophys. Res. Lett., **42**, 10773-10781.

Pace, M. L., I. Reche, J. J. Cole, A. Fernández-Barbero, I. P. Mazuecos, and Y. T. Prairie. 2012. pH change induces shifts in the size and light absorption of dissolved organic matter. Biogeochemistry **108**: 109–118.

Panneer Selvam, B., J.-F. Lapierre, A. R. A. Soares, D. Bastviken, J. Karlsson, and M. Berggren. 2019. Photo-reactivity of dissolved organic carbon in the freshwater continuum. Aquat. Sci. **81**: 57.

Raymond, P. A., and others. 2013. Global carbon dioxide emissions from inland waters. Nature, **503**, 355–359.

Seekell, D. A., J.-F. Lapierre, J. Ask, A.-K. Bergström, A. Deininger, P. Rodríguez, and J. Karlsson. 2015. The influence of dissolved organic carbon on primary production in northern lakes. Limnol. Oceanogr. **60**: 1276–1285.

Shen, F., Y. X. Zhou, and G. L. Hong. 2012. Absorption property of non-algal particles and contribution to Total light absorption in optically complex waters, a case study in Yangtze estuary and adjacent coast. Adv. Intell. Soft Comput. **141**: 61–66.

Suggett, D. J., O. Prášil, and M. A. Borowitzka. 2010. Chlorophyll a fluorescence in aquatic sciences: Methods and applications. Dordrecht, Netherlands: Springer.

Tassan, S., and G. M. Ferrari. 1995. An alternative approach to absorption measurements of aquatic particles retained on filters. Limnol. Oceanogr. **40**: 1358–1368.

Thrane, J.-E., D. O. Hessen, and T. Andersen. 2014. The absorption of light in lakes: Negative impact of dissolved organic carbon on primary productivity. Ecosystems **17**: 1040–1052.

Twardowski, M. S., E. Boss, J. M. Sullivan, and P. L. Donaghay. 2004. Modeling the spectral shape of absorption by chromophoric dissolved organic matter. Mar. Chem. **89**: 69–88.

Vachon, D., J.-F. Lapierre, and P. A. del Giorgio. 2016. Seasonality of photochemical dissolved organic carbon mineralization and its relative contribution to pelagic CO2 production in northern lakes. J. Geophys. Res. Biogeosci. **121**: 864–878.

Vähätalo, A. V., M. Salkinoja-Salonen, P. Taalas, and K. Salonen. 2000. Spectrum of the quantum yield for photochemical mineralization of dissolved organic carbon in a humic lake. Limnol. Oceanogr. **45**: 664–676.

Wanninkhof, R. 1992. Relationship between wind speed and gas exchange over the ocean. J. Geophys. Res. Oceans **97**: 7373–7382.

Weyhenmeyer, G., S. Kosten, M. Wallin, L. Tranvik, E. Jeppesen, and F. Roland. 2015. Significant fraction of CO_2 emissions from boreal lakes derived from hydrologic inorganic carbon inputs. Nat. Geosci. **8**: 933–936.

Williamson, C., R. Stemberger, D. Morris, and S. Paulsen. 1996. Ultraviolet radiation in North American lakes: Attenuation estimates from DOC measurements and implications for plankton communities. Limnol. Oceanogr. **41**: 1024–1034.

Williamson, C. E., E. P. Overholt, R. M. Pilla, T. H. Leach, J. A. Brentrup, L. B. Knoll, E. M. Mette, and R. E. Moeller. 2015. Ecological consequences of long-term browning in lakes. Sci. Rep. **5**: 18666.

Wozniak, B., and J. Dera. 2007. Light absorption in sea water. NY, USA: Springer.

Yang, H., T. Andersen, P. Dörsch, K. Tominaga, J.-E. Thrane, and D. O. Hessen. 2015. Greenhouse gas metabolism in Nordic boreal lakes. Biogeochemistry **126**: 211–225.

Acknowledgments

The study was funded by the Department of Biosciences, University Oslo, and two projects funded by the Research Council of Norway: COMSAT, grant 196336/S30 to T. Andersen and ECCO, grant 224779 to D.O. Hessen. We are most indebted to our colleagues in these projects.

Conflict of interest

None declared.

Submitted 26 November 2019
Revised 05 May 2020
Accepted 16 August 2020

Associate editor: David Antoine